Bias from H_2 Cleavage to Production and Coordination Changes at the Ni−Fe Active Site in the NAD^+-Reducing Hydrogenase from *Ralstonia eutropha*†

Simone Löscher,‡ Tanja Burgdorf,§ Ingo Zebger,|| Peter Hildebrandt,|| Holger Dau,‡ Bärbel Friedrich,§ and Michael Haumann*,‡

Freie Universität Berlin, Institut für Experimentalphysik, Arnimallee 14, D-14195 Berlin, Germany, Humboldt-Universität zu Berlin, Mikrobiologie, Chausseestrasse 117, D-10115 Berlin, Germany, and Technische Universität Berlin, Max-Volmer-Institut für Biophysikalische Chemie und Biochemie, Strasse des 17 Juni 135, D-10623 Berlin, Germany

Received May 30, 2006; Revised Manuscript Received August 3, 2006

ABSTRACT: The soluble NAD^+-reducing Ni−Fe hydrogenase (SH) from *Ralstonia eutropha* H16 is remarkable because it cleaves hydrogen in the presence of dioxygen at a unique Ni−Fe active site (Burgdorf et al. (2005) *J. Am. Chem. Soc. 127*, 576). By X-ray absorption (XAS), FTIR, and EPR spectroscopy, we monitored the structure and oxidation state of its metal centers during H_2 turnover. In NADH-activated protein, a change occurred from the $(CN)O_2Ni^{II}(\mu\text{-}S)_2Fe^{II}(CN)_3(CO)$ site dominant in the wild-type SH to a standard-like $S_2Ni^{II}(\mu\text{-}S)_2Fe^{II}(CN)_2(CO)$ site as the prevailing species in a specific mutant protein, HoxH−H16L. The wild-type SH primarily was active in H_2 cleavage. The nonstandard reaction mechanism does not involve stable EPR-detectable trivalent Ni oxidation states, namely, the Ni-A,B,C states as observed in standard hydrogenases. In the HoxH-mutant protein H16L, H_2 oxidation was impaired, but H_2 production occurred via a stable Ni−C state ($Ni^{III}-H^--Fe^{II}$), suggesting a reaction sequence similar to that of standard hydrogenases. It is proposed that reductive activation by NADH of both wild-type and H16L proteins causes the release of an oxygen species from Ni and is initiated by electron transfer from a [2Fe−2S] cluster in the HoxU subunit that at first becomes reduced by electrons from NADH. Electrons derived from H_2 cleavage, on the other hand, are transferred to NAD^+ via a different pathway involving a [4Fe−4S] cluster in HoxY, which is reducible only in wild-type SH but not in the H16L variant.

The cytoplasmic soluble Ni−Fe hydrogenase (SH)[1] plays an important role in energy conservation in the facultative aerobic, chemolithoautotrophic β-proteobacterium *Ralstonia eutropha* H16 as it catalyzes electron transfer from molecular hydrogen to NAD^+, thereby producing reducing equivalents for CO_2 fixation in the form of NADH (*1*). With regard to its primary sequence and cofactor content, the SH displays extensive similarities to NADH-ubiquinone-oxidoreductase (complex I) (*2*). As compared to the standard-type heterodimeric Ni−Fe hydrogenases (e.g., from *Desulfovibrio gigas*, which have been crystallized (*3*)), the SH is different in the following features (Figure 1).

(i) The SH consists of a hexameric $HoxHYUFI_2$ protein complex (*4*). The HoxHY module functions as a hydrogenase and the HoxFU module as a NADH-dehydrogenase (or diaphorase). The HoxH subunit carries the Ni−Fe active site, and the small HoxY subunit probably accommodates one

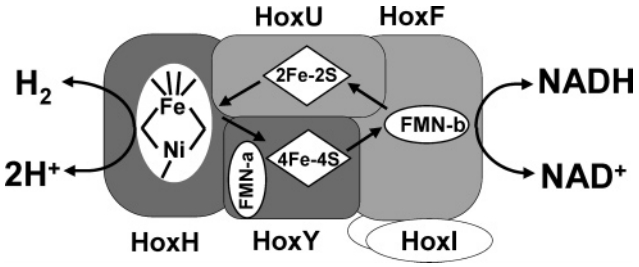

FIGURE 1: Scheme of the organization of the protein−cofactor complex of the soluble NAD-reducing Ni−Fe hydrogenase (SH) from *R. eutropha*. Only those Fe−S clusters are shown that presumably are involved in activation and catalysis on the basis this study. The HoxFU subunit (NADH-dehydrogenase) most likely carries additional Fe−S clusters (*8*). FMN-a, possibly bound to HoxY (*6*), is stabilized in the semiquinone state upon reduction (*16*).

[4Fe−4S] cluster proximal to the Ni−Fe site (*5*) and one FMN group (FMN-a) (*6*). The diaphorase part comprises further the [2Fe−2S] and [4Fe−4S] clusters (*5*), one FMN (FMN-b) (*7*), and the NAD^+ binding site (*8*). The sequence of electron-transfer steps from the Ni−Fe to the NAD binding site has not been elucidated yet. (ii) Hydrogen cleavage activity of the SH is highly insensitive to O_2 and CO (*9*) so that the SH is a promising candidate for H_2 biotechnological applications (*10*). (iii) In the oxidized state, the SH shows a unique structure of the Ni−Fe active site with five diatomic groups $(CN)O_3Ni(\mu\text{-}CysS)_2Fe(CN)_3(CO)$; both the Ni and the Fe atoms bind an extra CN molecule

† Financial support by the Deutsche Forschungsgemeinschaft within SFB-498 (Projects C1, C8, C9, and A8) is gratefully acknowledged.

* Corresponding author. Tel.: +49 30 8385 6101; fax: +49 30 8385 6299; e-mail: haumann@physik.fu-berlin.de.

‡ Freie Universität Berlin.

§ Humboldt-Universität zu Berlin.

|| Technische Universität Berlin.

[1] Abbreviations: DCIP, dichloroindophenol; EPR, electron paramagnetic resonance; EXAFS, extended X-ray absorption fine structure; FTIR, Fourier transform infrared spectroscopy; NAD^+/NADH, oxidized/reduced nicotinamid−adenine−dinucleotide; SH, NAD-reducing soluble hydrogenase; XANES, X-ray absorption near-edge structure; XAS, X-ray absorption spectroscopy.

10.1021/bi061068f CCC: $33.50
Published on Web 09/02/2006

(*11*, *12*). One O ligand at Ni may stem from a peroxidic species that blocks the access of H_2 in the oxidized state of the SH (*11*, *12*). It has been proposed that the other two terminal O ligands of Ni are derived from two of the four conserved cysteines present in the large subunit of all Ni−Fe hydrogenases (*8*, *12*), which are oxidized to sulfenates (CysSO) in the SH (*11*). (iv) An unprecedented mechanism of H_2 cleavage seems to operate in the SH, not involving stable EPR-detectable trivalent Ni oxidation states (*9*, *11*), namely, Ni-A/B with oxygen species bridging the Ni and Fe (*13*) and, more importantly, also not the Ni−C state as characterized by a hydride (H^-) in the bridging position between Ni^{III} and Fe^{II} (*14*, *36*). Instead, H_2 activation apparently takes place solely at the Ni (*11*).

A particularly interesting but barely understood feature of the Ni−Fe site of the SH is its structural flexibility. Under harsh and prolonged reducing conditions, the two sulfurs of thiol groups not directly coordinated to Ni in the oxidized enzyme become direct Ni ligands (*11*, *15*). Both the extra CN on the Ni and the Fe are lost (*11*). Thereby, a $(CysS)_4Ni$ site is formed that is similar to that of standard hydrogenases (*3*). The native SH in its oxidized state is inactive in H_2 cleavage. It can be rapidly activated by the addition of catalytic amounts of NADH, whereby an oxygen ligand at the Ni is removed, opening a binding site for H_2 (*11*). Recent studies by van der Linden et al. (*16*) have shown that under distinct reducing conditions (excess NADH and pH 6), a certain amount of the protein exhibits the EPR-visible Ni−C state of standard hydrogenases.

In this study, we have analyzed the structural and functional properties of a selected SH mutant protein carrying the His16Leu (H16L) exchange in the active site containing subunit HoxH. Histidine-16 is a conserved residue of the so-called L0 motif at the N-terminus of the large subunit widely conserved among energy converting Ni−Fe hydrogenases (*17*). In the *D. gigas* hydrogenase, the corresponding histidine residue (H20) is located at a distance of about 11 Å from the Ni−Fe site and the proximal [4Fe−4S] cluster in the small subunit, close to the interface between the two subunits (*3*). The SH−H16L mutant has a particularly interesting phenotype since it is almost inactive in H_2 oxidation but still able to catalyze hydrogen production.

MATERIALS AND METHODS

The wild-type and H16L mutant SH proteins of two independent preparations each were purified from *R. eutropha* and concentrated under aerobic conditions as described in ref *18*. Protein samples were degassed under N_2. For treatments in the presence of H_2, the atmosphere was exchanged by repeated degassing (*11*). Reductant stock solutions were freshly prepared (NADH, sodium-dithionite) in 20 mM Tris-HCl buffer, pH 8 and bubbled with nitrogen for 15 min. Samples finally contained concentrations of 25 μM or 10 mM NADH, or 10 mM dithionite, and protein concentrations of 1.01−1.28 mM, pH 8. After reductants were added, the samples were incubated at room temperature for 10 min, and then ~20 μL was filled under Ar atmosphere into specialized sample holders, which were immediately frozen in liquid nitrogen. The same samples were used for XAS and EPR measurements carried out before and after XAS. An aliquot of each sample was frozen separately for IR experiments.

Table 1: Relative Activities of Wild-Type (WT) and H16L Mutant Proteins of the SH

SH sample	addition of	activity
		H_2 cleavage (%)[a]
WT	NAD^+ 0.75 mM, H_2 45 μM	100
H16L		0.3
		H_2 production (%)[b]
WT	NADH 1.5 mM	100
H16L		6.8
WT	NADH 1.5 mM, FMN 2 μM	121
H16L		8.0
WT	NADH 1.5 mM,	127
H16L	sodium-dithionite 20 mM	9.1

[a] The absolute H_2 cleavage activity of WT as determined by the photometric assay was 60 U/mg (= 100%). [b] The absolute H_2 production activity of WT as determined by amperometry was 0.41 U/mg (= 100%).

Under aerobic conditions, H_2 cleavage activity was determined either with a Clark-type electrode (*11*) or by a photometric assay using either NAD^+ or benzyl viologen as an artificial electron acceptor in 50 mM Tris-HCl buffer, pH 8 (*18*), and H_2 production was assayed amperometrically using a Clark-type electrode in 50 mM phosphate buffer, pH 5.5. All buffers for amperometry were saturated with N_2 before use, but assay conditions were not strictly anaerobic.

EPR was performed in the laboratory of Prof. R. Bittl (Free University Berlin) on a Bruker Elexsys E580 spectrometer equipped with a helium cryostat (Oxford) (microwave frequency 9.41 GHz, modulation frequency 100 kHz, modulation amplitude 10 G). IR spectra were recorded on a Bruker IFS66VS spectrometer equipped with a photovoltaic MCT detector at a resolution of 2 cm^{-1} as in ref *19*. IR spectra were baseline corrected using the software available with the spectrometer. Atomic absorption spectroscopy was carried out in the laboratory of Dr. K. Irrgang at the Technical University Berlin as described in ref *19*. X-ray absorption spectroscopy (XAS) was performed at beamline D2 of the EMBL outstation (at HASYLAB, DESY, Hamburg, Germany). Fluorescence-detected XAS spectra at the nickel and iron K-edges were collected at 20 K as previously described (*11*, *19*) during two measuring periods. XAS spectra were averaged (six to 12 scans) after energy calibration of each scan (*11*, *19*) and normalized, and EXAFS oscillations were extracted as described in ref *20*. The energy scale of EXAFS spectra was converted to the *k*-scale using E_0 values of 8333 eV (Ni) and 7112 eV (Fe). Unfiltered k^3-weighted spectra were used for least-squares curve-fitting and for the calculation of Fourier transforms (FTs). The shown FTs represent *k*-values ranging from 2 to 13 $Å^{-1}$ (Ni EXAFS, up to 650 eV above E_0) and from 2 to 16 $Å^{-1}$ (Fe EXAFS, up to 1000 eV above E_0). EXAFS simulations (*11*, *19*) were performed using phase functions calculated with Feff-7 (*21*).

RESULTS

The SH−H16L mutant protein has been reported to form a stable hexameric complex, to incorporate Ni at the active site, and to display a D_2/H^+ exchange activity similar to the wild-type SH (WT) (*18*). Although the H_2 cleavage activity of H16L was found to be negligibly low, the H_2 production rate amounted to about 10% of the WT level if dithionite was used as an external electron donor (Table 1). Figure 2 shows that upon addition of NADH, H_2 is rapidly produced

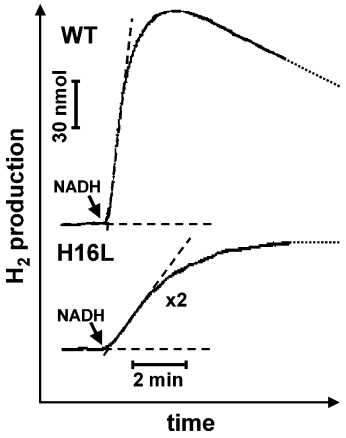

FIGURE 2: H_2 production of the wild-type (WT) and the H16L mutant protein of SH. Conditions: protein 1 nM and NADH 1.5 mM. Dashed lines denote the initial rate of H_2 production (for specific activities, see Table 1); dotted lines refer to the subsequent H_2 cleavage only in WT. The arrows mark the addition of NADH.

by WT, accompanied by NAD^+ formation, but came to a stop within ~2 min. Rate and yield were lower with H16L but continued over a period of >8 min. After these time intervals, the redox potential proportional to the NAD^+/NADH ratio in the assay mixture presumably becomes so positive that H_2 production no longer proceeds. That H_2 production was sustained for longer time periods in both enzymes exposed to the lower potential of 20 mM dithionite (not shown) corroborates this interpretation. Thereafter, only in WT, but not in H16L, the slower disappearance of the previously produced H_2 was observed (Figure 2). The apparent lower rate of H_2 cleavage in the WT protein, ca. 10% of the H_2 production activity, may point to different rate-limiting steps in Ni−Fe → NAD^+ and NADH → Ni−Fe electron transfer. The lower rate of initial H_2 production in H16L points to changes in the catalytic behavior. It is worth noting that we attribute the ~10% H_2 production activity to the main population of the (spectroscopically somewhat heterogeneous) H16L protein as this particular level of activity was well-reproducible in several independent preparations. In any event, the H16L derivative of the SH is able to produce H_2 at a significant rate and without subsequent consumption of the product.

To investigate whether the lesion in H_2 cleavage in H16L is due to changes at its Fe−S clusters, XAS at the Fe K-edge was performed. Fe XANES and EXAFS spectra of the oxidized WT and H16L proteins indicate that the Fe−S cluster complement is dominated by [4Fe−4S] clusters and is compatible with the presence of at least one further [2Fe−2S] cluster as proposed previously (*22*, *23*). The almost indistinguishable XAS spectra indicated a similar Fe−S cluster complement with respect to the structure and oxidation state in both enzymes (Figure 3, see legend). Hence, the lack of H_2 cleavage in H16L likely is not due to major changes at the Fe−S clusters.

The functioning of the redox cofactors in electron transfer was investigated by EPR. Spectra resulting from reduced Fe−S clusters in the two proteins obtained in the presence of NADH and H_2 (i.e., under conditions where autocatalytic activation of wild-type SH is achieved (*9*, *11*)) are different (Figure 4). Around $g = 1.94$ at 30 K, a split signal, presumably containing contributions from $[2Fe-2S]^+$ and

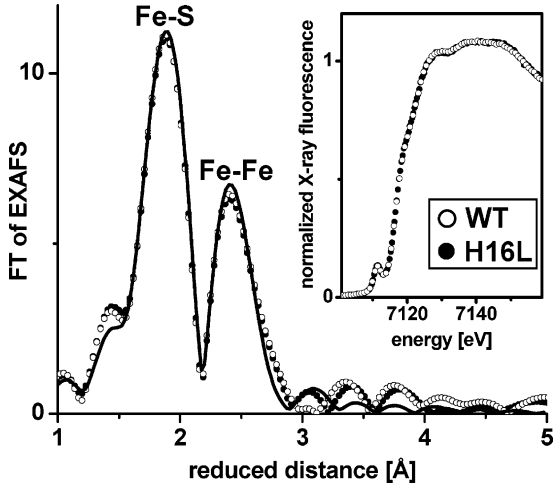

FIGURE 3: Fourier transforms of EXAFS oscillations at the Fe K-edge predominantly due to the Fe−S clusters in the oxidized SH proteins. Experimental data: open circles, wild-type (WT) and solid circles, H16L mutant protein. The line represents a simulation with two shells of Fe−backscatterer interactions with the following parameters (coordination number per Fe atom *N*/Fe−backscatterer distance *R*/Debye−Waller parameter $2\sigma^2$): shell I, Fe−S interactions, 3.9/2.26 Å/0.007 Å^2; shell II, Fe−Fe interactions, 2.6/2.72 Å/0.011 Å^2. The error factor (*35*) R_F was 9.7%. The value of the number of Fe−Fe interactions, $N_{II} = 2.6$, as well as the mean Fe−Fe distance of 2.72 Å are compatible with the presence of three to four [4Fe−4S] clusters (three Fe−Fe distances per Fe atom) and with at least one [2Fe−2S] cluster (one Fe−Fe distance per Fe atom) in both SH proteins. This result is in line with the content of 19 ± 2 Fe atoms per SH complex both in WT and in H16L preparations as determined by atomic absorption spectroscopy (data not shown). Inset: respective Fe K-edge spectra that are almost indistinguishable.

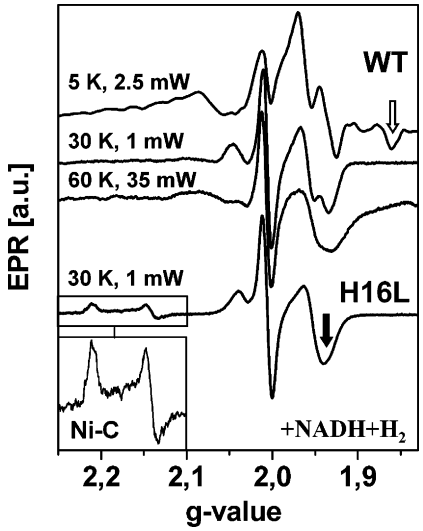

FIGURE 4: EPR spectra in the X-band of the SH proteins at the indicated microwave power and temperature settings in the presence of 25 μM NADH and 100% H_2. Open arrow, signal attributable to a $[4Fe-4S]^+$ cluster and solid arrow, signal attributable to a $[2Fe-2S]^+$ cluster. The inset shows an enlarged view of the Ni−C region of the spectrum of the H16L mutant. The narrow signal around $g = 2$ is due to the FMN• semiquinone radical(s); spectra were approximately normalized according to the latter signal for better comparison.

$[4Fe-4S]^+$ cluster(s) (*22*), is observed for WT, whereas H16L shows a nonsplit $[Fe-S]^+$ signal, suggesting the presence of only one type of reduced Fe−S cluster. At 5 K, the WT spectrum is dominated by the $[4Fe-4S]^+$ cluster as

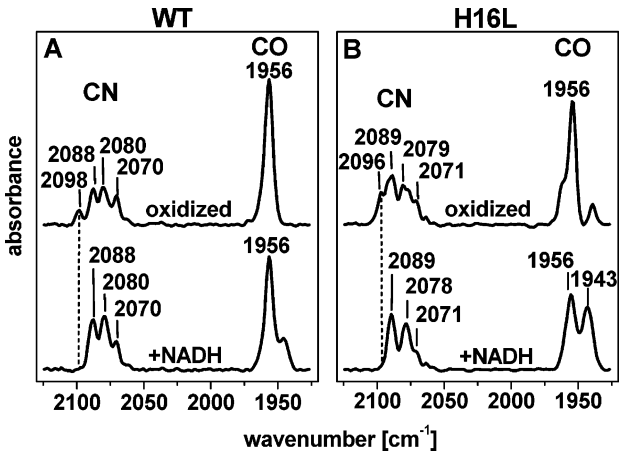

FIGURE 5: IR spectra in the C≡N and C≡O stretching vibration modes of (A) wild-type and (B) H16L protein of the SH in their oxidized (top) and NADH-reduced (bottom) forms. Spectra were normalized to about equal absorption of the whole CO band region.

indicated by a prominent signal at $g = 1.86$ due to the saturation of the $[2Fe-2S]^+$ signal at the high microwave power that has been employed. On the other hand, at 60 K, the spectrum largely reflects the $[2Fe-2S]^+$ cluster since the $[4Fe-4S]^+$ signal is almost invisible due to relaxation broadening (*22*, *23*). The shape of the $[Fe-S]^+$ signal of H16L was found to be independent of the microwave power and temperature and largely invariant toward the reducing conditions (i.e., reduction by NADH in the presence or absence of H_2 or by dithionite (data not shown)). Furthermore, no significant differences as compared to the 60 K $[Fe-S]^+$ spectrum of the WT protein were observed. On the basis of these findings, we propose that in H16L, external reductants are capable of reducing the [2Fe−2S] cluster but not the [4Fe−4S] clusters.

Interestingly, in (NADH + H_2)-reduced H16L (Figure 4) and in (NADH-only)-reduced H16L (not shown), a sizable EPR signal from the Ni−Fe site typical of the Ni−C state (*14*) is observed with g_x- and g_y-values of 2.21 and 2.14 (g_z could not be obtained because of the strong overlap of EPR signals from Fe−S clusters and $FMN^{\bullet}$ semiquinone radical(s) around $g = 2$) at a pH of 8. In the presence of dithionite, the Ni−C signal was smaller (not shown). In contrast, the Ni−C state could not be induced in WT under activating (+NADH) or autocatalytic conditions (+NADH + H_2) at pH 8. Oxidized WT and H16L are EPR-silent around $g = 2.3-2.1$ (not shown), suggesting the absence of the Ni-A/B oxidation states containing Ni^{III} (*14*) in both proteins. Formation of Ni-A/B requires binding of an oxygen species in a bridging position between Ni and Fe (*13*, *24*), whereas in the case of the Ni−C state, the bridging species is a hydride (*14*, *36*). The observation of a Ni−C signal at pH 8 only in H16L implies significant coordination changes in the environment of both Ni and Fe, at least for a portion of the protein preparation.

As a tentative interpretation of the EPR results, we suggest that the [4Fe−4S] cluster, which is not reduced in H16L, is the one presumably bound to the HoxY subunit (*8*), proximal to the Ni−Fe site. This Fe−S cluster seemingly cannot be reduced by external reductants as it was not reduced in the presence of NADH or dithionite in H16L. Apparently, its reduction is achieved only by electron transfer from the Ni−Fe site upon hydrogen cleavage because a reduced [4Fe−4S] cluster was observed in WT where this reaction is functional. On the other hand, the [2Fe−2S] cluster presumably located in HoxU (*8*) becomes reduced both in WT and in H16L. This cluster may be part of a different electron-transfer pathway from the NAD^+ binding site to the Ni−Fe site employed during reductive activation of the SH (vide infra).

IR spectroscopy was employed to monitor changes of the diatomic ligands at the Ni and Fe atoms (Figure 5). The presence of four dominant IR bands in the CN spectral region and of one band in the CO region in oxidized WT (Figure 5A) indicates the binding of three CN and one CO to the Fe and of one CN to the Ni (*9*, *11*, *12*) in contrast to the two CN and one CO ligation pattern at the Fe in standard hydrogenases (*25*). The four CN and the one CO stretching modes are also found in the oxidized H16L protein at nearly the same frequencies. However, H16L displays additional bands in the CO stretching region, and a more detailed inspection of the spectra reveals further bands in the CN stretching envelope. Thus, these findings suggest that the H16L sample contains (at least) two types of active sites. Whereas in one portion of the sample, the Ni−Fe center possesses essentially the same coordination pattern and active structure as the WT protein, for the remaining portion(s), the ligation pattern is modified. Such a heterogeneity, which is found to a much smaller extent in the WT preparation, can also account for the different relative intensities in the IR spectra of both enzymes. Upon reduction under activating conditions (+NADH), the prominent CO stretching bands of the WT and H16L proteins (1956 cm^{-1}) remain unchanged, and the bands around 2098 cm^{-1} shift to lower wavenumbers (*12*). However, for the mutant, a substantial loss in intensity is observed concomitant to considerable increase of the second CO stretching mode at 1943 cm^{-1} (Figure 5B). Such a low frequency CO band has been interpreted in terms of a reduced standard ligation pattern (i.e., no extra CNs at the Ni and the Fe (*16*)). This view is in line with the distinct intensity decrease of the CN band at 2071 cm^{-1}. Also, in the WT protein, a shoulder at ca. 1945 cm^{-1} with a relatively weak intensity is observed, indicating redox-linked coordinative changes of the active site, albeit in a much smaller fraction of the protein than for the H16L variant.

For both the WT and the H16L mutant, we have measured XAS spectra at the Ni K-edge to investigate the atomic structure of the Ni site. In the XANES region, information mainly on the ligands in the first coordination sphere of Ni is obtained (Figure 6). The large primary maximum of the Ni K-edge of ~1.5 and the absence of a pre-edge peak around 8336 eV in oxidized WT (solid arrow) indicates a nearly octahedral coordination of the Ni by two CysS, one CN, and three oxygen ligands as previously found (*11*). The smaller edge maximum and less steep edge slope in the NADH-activated WT reflects the loss of one oxygen species from Ni. It is replaced by a hydrogen species under autocatalytic conditions (NADH + H_2), giving rise to an increase in the edge maximum and to the resolved pre-edge peak at ~8336 eV (Figure 6) due to the enhancement of dipolar-forbidden 1s → 3d electronic transitions in the more asymmetrically coordinated Ni as discussed in ref *11*.

Already in the oxidized state of H16L the primary edge maximum is largely diminished, which immediately reveals

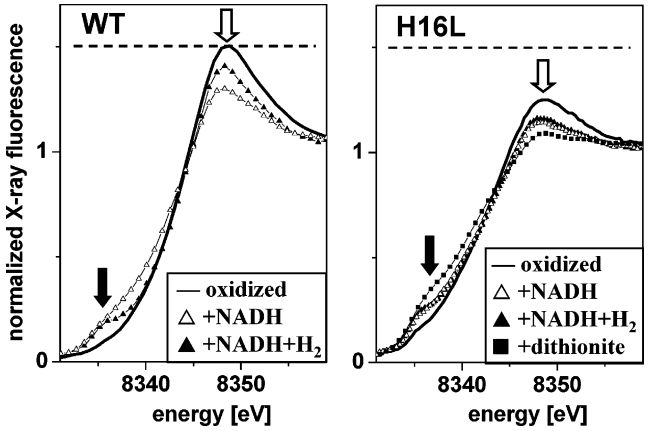

FIGURE 6: XANES spectra at the Ni K-edge of WT and H16L proteins under the indicated redox conditions. The open arrows denote the primary maximum of the K-edge; the solid arrows point to the peak features in the preedge region.

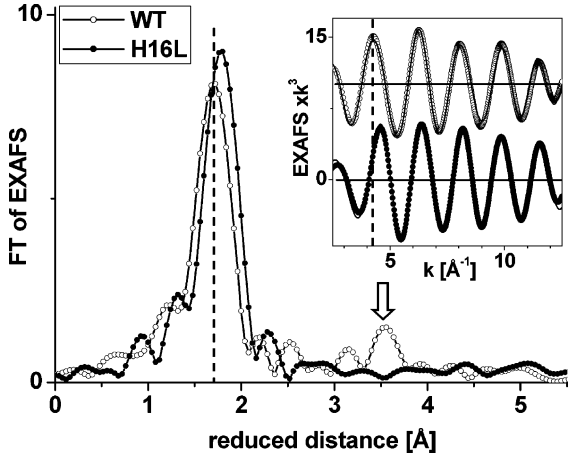

FIGURE 7: Fourier transforms of Ni EXAFS oscillations in the NADH-reduced SH proteins. The inset shows the backtransforms into the *k*-space of Fourier isolates from 1 to 2.5 Å of reduced distance. The lines in the inset represent simulations with parameters given in Table 2 (fit II). The open arrow points to the peak tentatively attributed to Ni−S vectors of about 3.5 Å length (*11*).

a coordination change at the Ni, most likely caused by the replacement of hard oxygen ligands by soft sulfurs from thiol groups of cysteines (*26*). For the NADH- and (NADH + H_2)-reduced H16L, the edge maximum was found to be even smaller, suggesting a similar coordination change as in the WT protein. Previously, it has been shown (*11*) that the presence of a sizable pre-edge peak at ~8336 eV is related to the presence of Ni-bound hydrogen species in the SH. As there is such a pre-edge peak under both the previous conditions in H16L, a hydrogen species seems to be bound to Ni even in the absence of externally added H_2. Further evidence for this view comes from the spectrum recorded in the presence of dithionite where the edge maximum is smaller and the pre-edge peak converts to a shoulder in the rising part of the edge, suggesting a decrease in energy of $1s \rightarrow 4p_z$ transitions in pentacoordinated Ni (Figure 6). Presumably, the stronger reductant induces further reduced states of the Ni in line with the EPR and FTIR results. The flat edge slope and the small maximum hardly exceeding unity in the dithionite-reduced enzyme strongly suggest the binding of four CysS to Ni in H16L (cf. ref *11*). The Ni XANES indicates a similar coordination change under activating reducing conditions in WT and H16L, namely, the loss of one oxygen ligand to open a hydrogen binding site at the Ni. In addition, the coordination pattern by cysteine seems to change in the activated enzymes to $(CysSO)_2$-$(CysS)_2$Ni in WT and $(CysS)_4$Ni in H16L (the attribution of the O ligands to sulfenates is tentative but based on conservative considerations; see ref *11*).

More quantitative information on the Ni site structures was obtained by the analysis of EXAFS spectra from NADH-activated enzymes (Figure 7). The primary peak in the FT of EXAFS oscillations from H16L is clearly shifted to larger distances pointing to the prevalence of longer Ni−S vectors over shorter Ni−(O,C) vectors in H16L, which is in contrast to the opposite tendency observed for the WT protein. Accordingly, EXAFS simulations using only two coordination shells yielded a lower coordination number of the (O,C) shell but a higher coordination number of the sulfur shell in H16L as compared to WT (Table 2, fit I). A more elaborated simulation approach (fit II) takes into account the CN ligand at Ni as detected by IR spectroscopy, the Ni−Fe distance, and splitting of the sulfur shell into two shells to account for two different Ni−S bond lengths (*27*). Such a fit reveals the presence of one CN, two oxygen, and two CysS ligands at Ni in the WT protein, as previously described (*11*), whereas the simulation of the spectrum of H16L requires four CysS ligands and, optionally, one CN in accordance with the XANES spectra. In line with these results, the FT peak at ~3.5 Å in the EXAFS spectrum of the WT protein, which also has been observed previously (*11*) and attributed to the S atoms of the two cysteines that do not bind via their S atoms to Ni (*11*), is absent in H16L (Figure 7). The XANES and EXAFS, therefore, allow the conclusion that the two CysS groups that presumably are more remote from Ni in the WT become direct Ni ligands in H16L, resulting in a $(CysS)_4$Ni site in NADH-activated H16L that is similar to that of standard hydrogenases.

DISCUSSION

Comparison of the WT and H16L mutant affords new information on structural and functional properties of the particularly complex NAD-reducing Ni−Fe hydrogenase from *R. eutropha* H16 (Figure 8). In the WT, we observed reduction of at least two Fe−S clusters that are proposed to correspond to a [4Fe−4S] cluster putatively bound to the HoxY subunit in a proximal position to the Ni−Fe site and to a [2Fe−2S] cluster in HoxU. In H16L, however, only the [2Fe−2S] cluster was reduced. These findings provide first evidence for two different electron-transfer pathways in the SH. The [2Fe−2S] cluster seems to be part of the electron-transfer chain from NADH to the Ni−Fe site upon reductive activation of the enzyme. This pathway is functional in both WT and H16L. On the other hand, the [4Fe−4S] cluster seems to be involved predominantly in electron transfer from the Ni−Fe site to NAD^+ operating in the direction of H_2 cleavage. This pathway is active in WT but not in H16L. Midpoint potentials of about −325 mV for the [2Fe−2S] cluster and of less than or equal to −445 mV for the [4Fe−4S] cluster(s) at pH 8 have been reported previously (*22*). Consequently, activation with NADH (reduction potential of ca. −350 mV at pH 8) cannot reduce the [4Fe−4S] cluster. Thus, only the [2Fe−2S] cluster (and the

Table 2: Simulation Parameters of EXAFS Oscillations at the Ni K-Edge of NADH-Reduced Proteins[a]

preparation	shell	N_i (per Ni)	R_i (Å)	$2\sigma^2_i$ (Å^2)	R_F (%)
WT + NADH	C	−/1#	−/1.98	−/0.002#	13.5&/10.5
	O	3.3§/2#	2.03/2.03	0.015*/0.004	
	S	1.7§/1#	2.21/2.25	0.008*/0.003	
	S	−/1#	−/2.47	−/0.006	
	Fe	−/1#	−/2.56	−/0.013	
H16L + NADH	C	−/1#	−/1.82	−/0.002#	13.5&/8.9
	(O,C)/O	1.6§/−	2.15/−	0.015*/−	
	S	3.4§/3#	2.18/2.17	0.008*/0.009	
	S	−/1#	−/2.58	−/0.008	
	Fe	−/1#	−/2.63	−/0.015	

[a] N_i, coordination numbers; R_i, Ni−backscatterer distances; and $2\sigma^2_i$, Debye−Waller parameters. Two sets of parameters (fit I/fit II) are shown, corresponding to a joint simulation (*34*) of the two spectra (fit I) using two backscatterer shells and to simulations of the individual spectra (fit II) using five backscatterer shells. The following restrains were used in the simulations: #, parameter fixed at the given value; §, the sum of the coordination numbers of shells 1 and 2 was set to a value of 5; *, the respective Debye−Waller parameters were coupled in the joint simulation to yield equal values for both spectra; and &, R_F value for the joint fit. The error sums (R_F) (*35*) were calculated for reduced distances ranging from 1 to 3 Å. R_F represents the deviation between the backtransform into the *k*-space of the Fourier transformed experimental spectrum between 1 and 3 Å and the simulated spectrum in percent (*35*). The error of the derived distances R_i is estimated as being about ±0.02 Å; the uncertainty in $2\sigma^2$ is about 50% of the given values for best-fit results.

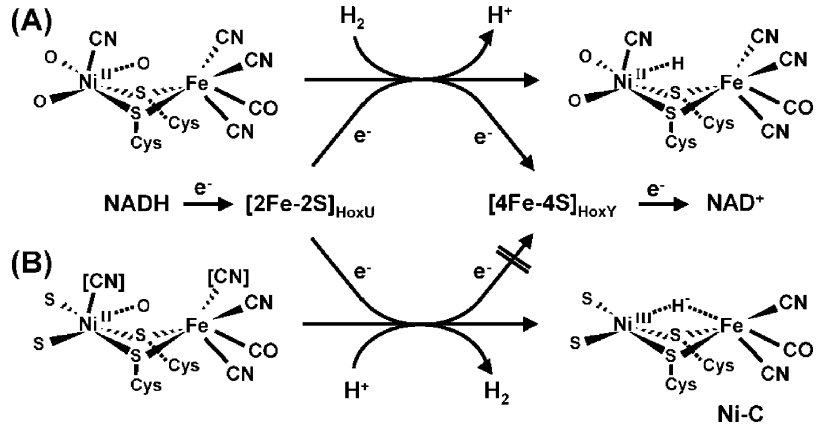

FIGURE 8: Summary of the structural features of the Ni−Fe site and of its changes upon the activation process in the two SH variants. Oxygen species and CN molecules that leave the metal site are not displayed for clarity. (A) In the oxidized wild-type SH (left), two CN molecules not found in standard hydrogenases are present, and two O ligands instead of S are bound to Ni. Activation upon electron flow from NADH via the [2Fe−2S] cluster to the Ni−Fe site in the presence of H_2 involves exchange of the third O ligand against a H species at Ni. H_2 cleavage is the prevailing reaction and generates electron flow from the Ni−Fe site via a [4Fe−4S] cluster to NAD^+. (B) In the H16L protein already in its oxidized state (left), two O ligands at Ni largely are exchanged against S. The additional two CN molecules, [CN], are present only in part of the preparation, and further portions are lost upon activation that involves the loss of an O ligand from Ni as in WT. Because subsequent electron transfer to the [4Fe−4S] cluster is impaired in the major portion of the protein containing a standard-like $(CysS)_4Ni-Fe(CN)_2(CO)$ site after activation, the dominant reaction in H16L is H_2 production, involving a typical Ni−C state. Minor populations of species displayed in panel B may be found also in WT protein, and species shown in panel A may appear as admixtures also in H16L preparations.

FMN molecule(s)) seems to be relevant for electron transfer to the Ni−Fe site during reductive activation.

At least three options may explain the lack of electron-transfer Ni−Fe → [4Fe−4S] in H16L. (i) The redox potential of the Ni−Fe site is increased due to the observed metal coordination changes. Then, only H_2 production from NADH should remain functional, similar to standard hydrogenases where the potential of the proximal [4Fe−4S] cluster is only about −300 mV (*28*) such that only H_2 production proceeds under reducing conditions (*29*). (ii) The potential of the [4Fe−4S] cluster is lowered. In analogy to structural data of standard hydrogenases, the H16L mutation may be rather remote from Ni−Fe (~11 Å), but substitution of His-16 (His-20 in the *D. gigas* hydrogenase) in the conserved L0 motif of HoxH may affect the hydrogen bond network between the Ni−Fe site and the proximal Fe−S cluster and alter its potential. (iii) Structural changes due to the mutation may have canceled optimal π-orbital coupling for effective electron tunneling between the two redox centers. Which one of these options actually applies remains to be elucidated. In the SH, a second FMN (FMN-a), possibly bound to the HoxY subunit, has been proposed to be involved in H_2 cleavage (*6*). FMN-a is easily lost under reducing conditions. However, H_2 cleavage and production activity of H16L were not enhanced upon addition of FMN. Accordingly, there is no evidence that the lack of H_2 cleavage is caused by the absence of FMN-a in H16L.

The variability of the Ni−Fe site with respect to the number of CN ligands and Ni-coordinating sulfurs from cysteine is a striking feature of the SH. We observed that Ni binds two cysteine sulfurs in H16L, which presumably are not bound to the Ni of the WT protein. These two of the four conserved cysteines may be oxidized to sulfenates (CysSO) and bind to Ni via their O atoms (*11*, *16*). Support for such an assignment comes from recent crystallography data on the oxidized Ni-A,B states of *D. gigas* Ni−Fe hydrogenase (*13*) where also sulfenates are found and one binds to the Ni via its sulfur whereas the second bridges the

Ni and the Fe by coordination through its O and S atom, respectively. In the SH, such a bridging sulfenate is less likely in both WT and H16L since the stretching frequencies of the CN and CO ligands at the Fe are consistent with two bridging thiol groups. Accordingly, in the WT enzyme, two of the terminal oxygen ligands of Ni may stem from sulfenates of Cys-458 and Cys-62 in the HoxH subunit (*11*). In H16L, either the unmodified cysteines are present or the sulfenates now bind to the Ni via their S atoms.

Activation of oxidized WT and H16L proteins is achieved within seconds after adding superstoichiometric amounts of NADH or under autocatalytic conditions (substoichiometric concentrations of NADH under H_2 atmosphere) (*9*, *11*, *12*). The primary event of the activation process is the loss of an oxygen ligand at the Ni (ref *11* and this paper). Activation of standard hydrogenases from the inactive unready state (Ni-A) also requires the reductive removal of an oxygen species (peroxide) that is bound in a Ni−Fe bridging position (*13*). However, this activation process takes hours (*30*). More rapid activation of the SH may result from binding of the oxygen ligand not in a bridging but in a terminal position at Ni as inferred from the hexacoordinated configuration of Fe in the WT and H16L oxidized proteins. This seems to be valid also for those protein fractions possessing a standard hydrogenase ligation-type at the active site since no Ni-A state could be detected by EPR.

Thus, the prevailing NADH-activated form in the WT is attributed to a $(CN)O_2Ni^{II}(\mu\text{-}S)_2Fe^{II}(CN)_3(CO)$ configuration (the O ligands may stem from Cys-SO), whereas in the H16L variant, the standard-like $S_2Ni^{II}(\mu\text{-}S)_2Fe^{II}(CN)_2(CO)$ form coexists with portions where one or both of the extra CN ligands, [CN], in portions of the oxidized state are still bound (Figure 8). The H16L exchange may hamper stoichiometric incorporation of the additional cyanides during maturation, and/or they may be lost more easily during the purification procedure or reductive treatments then in WT protein where standard Ni−Fe sites containing fractions under certain conditions also are found (*16*). The SH fractions of the WT and the H16L protein with standard-like metal ligation exhibit a Ni−C EPR signal under distinct reductive conditions (ref *16* and this paper), but this state was not achievable in inactive SH preparations (*11*). It is worth noting that the presence of a transient state similar to Ni−C, which does not enrich during catalysis to an amount sufficient for detection by EPR, may not completely be ruled out also in wild-type SH. However, only for the H16L variant, formation of a stable Ni−C state seems to be correlated with H_2 production.

The H_2 cleavage activity of SH becomes oxygen sensitive when the Ni-bound CN is absent. It can be selectively removed by biochemical treatments of purified enzyme (*12*). Isolating the SH from a strain lacking the HypX maturation protein also yields an O_2-sensitive enzyme (*31*), the Ni-bound CN is absent, but Ni coordination by only two thiols and three oxygens as in WT appears to be retained (*32*). In the I64A (HoxH) protein that lacks the Ni-bound CN, but seemingly exhibits the same Ni coordination as the HypX deletion mutant, the oxidized enzyme could not be activated at all (*11*). In summary, the loss of the CN ligand of the Ni alone strongly increases the binding affinity for oxygen at the expense of the affinity for hydrogen. However, only the loss of the extra CN ligands of both Ni and Fe and the coordination of additional S atoms to Ni as in H16L seems to enable binding of a Ni−Fe bridging hydride to yield the stable EPR-detectable Ni−C state.

Because of the hexacoordinated Fe, the reactions of H_2 must be restricted to the Ni site in the wild-type SH protein. Thus, the underlying mechanism presumably is different from that of standard hydrogenases. Further investigations are required to elucidate the catalytic cycle. On the other hand, H_2 formation in the fraction of the H16L protein that possesses a standard-like ligation of the active site may occur via a more conventional reaction path (*33*) that, however, appears to be less sensitive to inhibition by dioxygen. Accordingly, genetically engineered SH proteins, inactive in H_2 oxidation, but being able to generate H_2 at moderately reducing potentials and in the presence of oxygen, are interesting candidates for future biotechnological applications.

ACKNOWLEDGMENT

We thank the staff at the EMBL beamline D2 (DESY, Hamburg) and in particular Dr. W. Meyer-Klaucke for excellent support. We are indebted to Prof. R. Bittl (FU-Berlin) for generous help with the EPR measurements and Dr. K. Irrgang (TU-Berlin) for support in AAS.

REFERENCES

1. Schneider, K., and Schlegel, H. G. (1976) Purification and properties of soluble hydrogenase from *Alcaligenes eutrophus* H 16, *Biochim. Biophys. Acta 452*, 66−80.
2. Albracht, S. P., and Hedderich, R. (2000) Learning from hydrogenases: location of a proton pump and of a second FMN in bovine NADH-ubiquinone oxidoreductase (Complex I), *FEBS Lett. 485*, 1−6.
3. Volbeda, A., Charon, M. H., Piras, C., Hatchikian, E. C., Frey, M., and Fontecilla-Camps, J. C. (1995) Crystal structure of the nickel−iron hydrogenase from *Desulfovibrio gigas*, *Nature 373*, 556−557.
4. Burgdorf, T., van der Linden, E., Bernhard, M., Yin, Q. Y., Back, J. W., Hartog, A. F., Muijsers, A. O., de Koster, C. G., Albracht, S. P., and Friedrich, B. (2005) The soluble NAD^+-reducing [NiFe]-hydrogenase from *Ralstonia eutropha* H16 consists of six subunits and can be specifically activated by NADPH, *J. Bacteriol. 187*, 3122−3132.
5. Massanz, C., Schmidt, S., and Friedrich, B. (1998) Subforms and in vitro reconstitution of the NAD-reducing hydrogenase of *Alcaligenes eutrophus*, *J. Bacteriol. 180*, 1023−1029.
6. Van der Linden, E., Bart, W., Faber, B., Bleijlevens, B., Burgdorf, T., Bernhard, M., Friedrich, B., and Albracht, S. P. J. (2004) Selective release and function of one of the two FMN groups in the cytoplasmic NAD^+-reducing [NiFe]-hydrogenase from *Ralstonia eutropha*, *Eur. J. Biochem. 271*, 801−808.
7. Schneider, K., and Schlegel, H. G. (1978) Identification and quantitative determination of the flavin component of soluble hydrogenase from *Alcaligenes eutrophus*, *Biochem. Biophys. Res. Commun. 84*, 564−571.
8. Tran-Betcke, A., Warnecke, U., Böcker, C., Zaborosch, C., and Friedrich, B. (1990) Cloning and nucleotide sequences of the genes for the subunits of NAD-reducing hydrogenase of *Alcaligenes eutrophus* H16, *J. Bacteriol. 172*, 2920−2929.
9. Happe, R. P., Roseboom, W., Egert, G., Friedrich, C. G., Massanz, C., Friedrich, B., and Albracht, S. P. J. (2000) Unusual FTIR and EPR properties of the H_2-activating site of the cytoplasmic NAD-reducing hydrogenase from *Ralstonia eutropha*, *FEBS Lett. 466*, 259−263.
10. Lutz, B. J., Fan, Z. H., Burgdorf, T., and Friedrich, B. (2006) Hydrogen sensing by enzyme-catalyzed electrochemical detection, *Anal. Chem. 77*, 4969−4975.
11. Burgdorf, T., Löscher, S., Liebisch, P., Van der Linden, E., Galander, M., Lendzian, F., Meyer-Klaucke, W., Albracht, S. P., Friedrich, B., Dau, H., and Haumann, M. (2005) Structural and oxidation-state changes at its nonstandard Ni−Fe site during

activation of the NAD-reducing hydrogenase from *Ralstonia eutropha* detected by X-ray absorption, EPR, and FTIR spectroscopy, *J. Am. Chem. Soc. 127*, 576−592.
12. Van der Linden, E., Burgdorf, T., Bernhard, M., Bleijlevens, B., Friedrich, B., and Albracht, S. P. J. (2004) The soluble [NiFe]-hydrogenase from *Ralstonia eutropha* contains four cyanides in its active site, one of which is responsible for insensitivity towards oxygen, *J. Biol. Inorg. Chem. 9*, 616−626.
13. Volbeda, A., Martin, L., Cavazza, C., Matho, M., Faber, B. W., Roseboom, W., Albracht, S. P., Garcin, E., Rousset, M., and Fontecilla-Camps, J. C. (2005) Structural differences between ready and unready oxidized states of [NiFe]-hydrogenases, *J. Biol. Inorg. Chem. 10*, 239−249.
14. Brecht, M., Van Gastel, M., Buhrke, T., Friedrich, B., and Lubitz, W. (2003) Direct detection of a hydrogen ligand in the [NiFe] center of the regulatory H2-sensing hydrogenase from *Ralstonia eutropha* in its reduced state by HYSCORE and ENDOR spectroscopy, *J. Am. Chem. Soc. 125*, 13075−13083.
15. Müller, A., Erkens, A., Müller, A., Schneider, K., Nolting, H.-F., Solé, V. A., and Henkel, G. (1997) NADH-induced changes of the nickel coordination within the active site of the soluble hydrogenase from *Alcaligenes eutrophus*: XAFS investigations on three states distinguishable by EPR spectroscopy, *Angew. Chem. 106*, 1812−1815.
16. Van der Linden, E., Burgdorf, T., de Lacey, A. L., Buhrke, T., Scholte, M., Fernandez, V. M., Friedrich, B., and Albracht, S. P. J. (2006) An improved purification procedure for the soluble [NiFe]-hydrogenase of *Ralstonia eutropha*: new insights into its (in)stability and spectroscopic properties. *J. Biol. Inorg. Chem. 11*, 247−260.
17. Massanz, C., and Friedrich, B. (1999) Amino acid replacements at the H_2-activating site of the NAD-reducing hydrogenase from *Alcaligenes eutrophus*, *Biochemistry 38*, 14330−14337.
18. Burgdorf, T., DeLacey, A. L., and Friedrich, B. (2002) Functional analysis by site-directed mutagenesis of the NAD(+)-reducing hydrogenase from *Ralstonia eutropha*, *J. Bacteriol. 184*, 6280−6288.
19. Buhrke, T., Löscher, S., Lenz, O., Schlodder, E., Zebger, I., Andersen, L. K., Hildebrandt, P., Meyer-Klaucke, W., Dau, H., Friedrich, B., and Haumann, M. (2005) Reduction of unusual iron−sulfur clusters in the H_2-sensing regulatory Ni−Fe hydrogenase from *Ralstonia eutropha* H16, *J. Biol. Chem. 280*, 19488−19495.
20. Dau, H., Liebisch, P., and Haumann, M. (2003) X-ray absorption spectroscopy to analyze nuclear geometry and electronic structure of biological metal centers−potential and questions examined with special focus on the tetranuclear manganese complex of oxygenic photosynthesis, *Anal. Bioanal. Chem. 376*, 562−583.
21. Zabinsky, S. I., Rehr, J. J., Aukudinov, A., Albers, R. C., and Eller, M. J. (1995) Multiple-scattering calculations of X-ray-absorption spectra, *Phys. Rev. B 52*, 2995−3009.
22. Schneider, K., Cammack, R., Schlegel, H. G., and Hall, D. O. (1979) The iron−sulphur centers of soluble hydrogenase from *Alcaligenes eutrophus*, *Biochim. Biophys. Acta 578*, 445−461.
23. Erkens, A., Schneider, K., and Müller, A. (1996) The NAD-linked soluble hydrogenase from *Alcaligenes eutrophus* H16: detection and characterization of EPR signals deriving from nickel and flavin, *J. Biol. Inorg. Chem. 1*, 99−110.
24. Carepo, M., Tierney, D. L., Brondino, C. D., Yang, T. C., Pamplona, A., Telser, J., Moura, I., Moura, J. J., and Hoffman, B. M. (2002) 17O ENDOR detection of a solvent-derived Ni−(OH(x))−Fe bridge that is lost upon activation of the hydrogenase from *Desulfovibrio gigas*, *J. Am. Chem. Soc. 124*, 281−286.
25. Happe, R. P., Roseboom, W., Pierik, A. J., Albracht, S. P. J., and Bagley, K. A. (1997) Biological activation of hydrogen, *Nature 385*, 126.
26. Colpas, G. J., Maroney, M. J., Bagyinka, C., Kumar, M., Willis, W. S., Suib, S. L., Mascharak, P. K., and Baidya, N. (1991) X-ray spectroscopic studies of nickel complexes, with application to the structure of nickel sites in hydrogenases, *Inorg. Chem. 30*, 920−928.
27. Gu, W., Jacquamet, L., Patil, D. S., Wang, H. X., Evans, D. J., Smith, M. C., Millar, M., Koch, S., Eichhorn, D. M., Latimer, M., and Cramer, S. P. (2003) Refinement of the nickel site structure in *Desulfovibrio gigas* hydrogenase using range-extended EXAFS spectroscopy, *J. Inorg. Biochem. 93*, 41−51.
28. Teixeira, M., Moura, I., Xavier, A. V., Moura, J. J., LeGall, J., DerVartanian, D. V., Peck, H. D., Jr., and Huynh, B. H. (1989) Redox intermediates of *Desulfovibrio gigas* [NiFe]-hydrogenase generated under hydrogen. Mössbauer and EPR characterization of the metal centers, *J. Biol. Chem. 264*, 16435−16450.
29. De Lacey, A. L., Moiroux, J., and Bourdillon, C. (2000) Simple formal kinetics for the reversible uptake of molecular hydrogen by [Ni−Fe] hydrogenase from *Desulfovibrio gigas*, *Eur. J. Biochem. 267*, 6560−6570.
30. De Lacey, A. L., Pardo, A., Fernandez, V. M., Dementin, S., Adryanczyk-Perrier, G., Hatchikian, E. C., and Rousset, M. (2004) FTIR spectroelectrochemical study of the activation and inactivation processes of [NiFe]-hydrogenases: effects of solvent isotope replacement and site-directed mutagenesis, *J. Biol. Inorg. Chem. 9*, 636−642.
31. Bleijlevens, B., Buhrke, T., van der Linden, E., Friedrich, B., and Albracht, S. P. (2004) The auxiliary protein HypX provides oxygen tolerance to the soluble [NiFe]-hydrogenase of *Ralstonia eutropha* H16 by way of a cyanide ligand to nickel, *J. Biol. Chem. 279*, 46686−46691.
32. Bleijlevens, B. (2002) Activation and sensing of hydrogen in nature. Ph.D. Thesis, University of Amsterdam, Amsterdam, The Netherlands.
33. Cammack, R., Robson, R., and Frey, M., Eds. (1997) *Hydrogen as a fuel: Learning from nature*; Taylor and Francis: London, UK.
34. Pospisil, P., Haumann, M., Dittmer, J., Sole, V. A., and Dau, H. (2003) Stepwise transition of the tetramanganese complex of photosystem II to a binuclear $Mn_2(\mu\text{-}O)_2$ complex in response to a temperature jump: a time-resolved structural investigation employing X-ray absorption spectroscopy, *Biophys. J. 84*, 1370−1380.
35. Meinke, C., Sole, V. A., Pospisil, P., and Dau, H. (2000) Does the structure of the water-oxidizing photosystem II−manganese complex at room temperature differ from its low-temperature structure? A comparative X-ray absorption study, *Biochemistry 39*, 7033−7040.
36. Foerster, S., van Gastel, M., Brecht, M., and Lubitz, W. (2005) An orientation-selected ENDOR and HYSCORE study of the Ni−C active state of *Desulfovibrio vulgaris* Miyazaki F hydrogenase, *J. Biol. Inorg. Chem. 10*, 51−62.

BI061068F